ARTICLES

Origin of mist and hackle patterns in brittle fracture

A. Rabinovitch and G. Belizovsky
Department of Physics, Ben-Gurion University, Beer Sheva 84105, Israel

D. Bahat
Department of Geology & Environmental Sciences, The Deichmann, Rock Mechanics Laboratory of the Negev, Ben Gurion University, Beer Sheva 84105, Israel

(Received 8 April 1999; revised manuscript received 29 November 1999)

A velocity growth rule for secondary cracks in brittle materials is suggested. This rule agrees with the assumption that the mist-hackle transition originates from the inability of the primary crack to overtake secondary cracks. The geometrical shapes of the secondary cracks in the mist and hackle zones change gradually with distance from the fracture origin. The velocity rule is used to calculate these shapes across the mist and at the beginning of the hackle zone. These calculations are shown to be in agreement with experimental results.

I. INTRODUCTION

One of the methods to determine fracture properties, either in their brittle or their ductile modes, is to analyze their surface morphology. While the morphology of brittle fracture surfaces has been known for many years,[1] a complete understanding of the physical processes leading to the observed patterns is still missing.

Surface morphologies (fracture markings) are ubiquitous on almost all fracture surfaces and particularly occur in various shapes and styles in brittle and semibrittle materials, including silicate glasses,[2,3] ceramics,[4,5] single crystals like quartz,[6] sapphire,[7] germanium,[8] and diamond,[9] metals like steel,[10] vitreous carbon,[11] transparent polymers (like PMMA),[12,13] and resins.[14] Fracture markings were also identified in nonbrittle materials, like jellies[15] and rubber.[16] Fractography analyses the causes and mechanisms of fracture via the characterization of fracture surface morphology in materials.

Fractography handles surfaces as small as several micrometers (fractured fibers) that can be examined only by scanning electron microscopy (SEM) or optical microscopy[3] and as large as 100 m (geological exposures). Most morphologies in the above-mentioned materials can be seen either by the naked eye or by a simple magnifying glass. Under ideal fracture conditions fractography displays some ten distinct morphological markings [Fig. 1(a)]. However, in reality only two to four markings appear.

There is a difference in morphology between cracks obtained under pure tension and cracks obtained under a combination of tension (mode I) and shear (so-called modes II and III). We concentrate here on pure mode I but for the sake of completeness mention also the other morphologies. *Striae* describe the fracture appearance that results from the combined modes I and III, and are manifested by elongated lines which are parallel to the direction of crack propagation. The location of the fracture origin can usually be identified as the locus where radial striae meet (originate). Concentric *undulations*, which form by mixed modes I and II, define the front on the fracture surface and are commonly convex towards

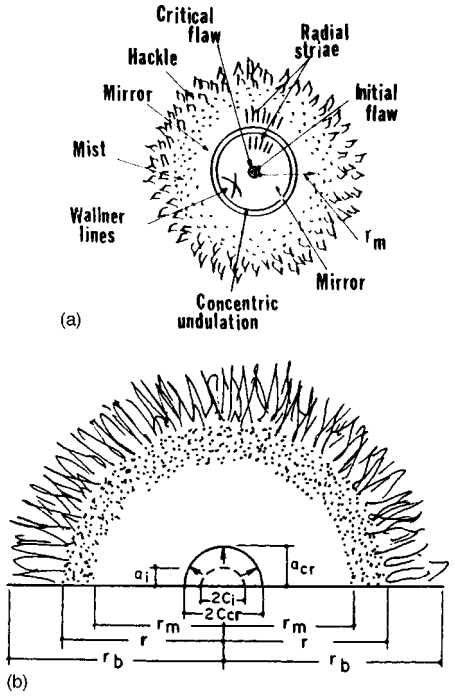

FIG. 1. (a) Schematic representation of a fracture surface showing the fracture origin at the initial flaw, the mirror plane, radial striae, concentric undulations, Wallner lines, mist, hackle, and the mirror radius r_m. (b) The usual brittle crack morphology (schematic). Shown are initial flaw length $2C_i$, critical flaw length $2C_{\rm cr}$, the mirror radius r_m (mirror-mist boundary), the mist radius r (mist-hackle boundary), and the hackle radius r_b (initiation of crack branching).

the direction of fracture propagation [Fig. 1(a)]. *Wallner lines* are very delicate curves that enable the measurement of crack velocity. These lines arise from the interaction of the fracture itself and the acoustic waves that accompany it. The curvatures of Wallner lines change with the ratio of crack velocity to the speed of sound. Kerkhof[17] gives the ranges of crack velocities and stress intensity factors at which Wallner lines are produced in glass as follows: $10\ \mathrm{m/s} \leqslant V \leqslant 1500\ \mathrm{m/s}$ and $27\ \mathrm{N\,mm^{3/2}} \leqslant K_I \leqslant 68\ \mathrm{N\,mm^{3/2}}$.

In a usual crack morphology of brittle materials, several zones appear in a sequence: the *initial flaw* is followed by the *critical flaw*, which in turn develops into the *mirror*. The *mist* and *hackle* zones appear in logical succession[15,18] followed by *crack branching*.[1,18] The mirror is a smooth surface which reflects light (hence the name). The mist, which is our main interest in this paper, consists of fine-scale secondary cracks which develop because of the stress field at the tip of the primary crack. Its name is due to the misty appearance of this zone. The hackle has a ''feathery''-like appearance, where roughening of the secondary cracks occurs. Crack branching occurs at the outside boundary of the hackle zone[19] [Figs. 1(a) and 1(b)].

The fracture plane extends from the critical flaw C_{cr} to three differently defined radii r_m (the mirror-mist boundary), r (the mist-hackle boundary), and r_b (initiation of macroscopic crack branching).[20]

The realization that the stippled perimeter of the smooth mirror surface, termed ''mist,'' defines the mirror boundary [Fig. 1(b)] sets the way for the estimation[21] of fracture stress by fractography. Terao[22] observed that the breaking stress varied quite consistently with the reciprocal of the square root of the mirror radius [Fig. 1(b)]. Many investigators have obtained the semiempirical formula of $\sigma_f r_j^{1/2} = A_j$, where σ_f is the fracture remote stress, r_j is the distance to a particular boundary, and A_j is a corresponding constant.

Very few studies considered the geometries of the secondary cracks in the mist zone and their significance. Johnson and Holloway[23] suggested to identify two distinct types of microcrack in the mist zone on the fracture surfaces of soda-lime silicate glass. One type predominates near the mirror boundary, and the other is concentrated near the hackle boundary. Ball *et al.*[24] studied the mist region in a series of soda-lime silica float glasses. They found the width of the mist region, W_{mist}, to be inversely related to the square of σ_f, which fits the mathematical prediction of the former equation, $W_{\mathrm{mist}} = r^2 - r_m^2 = (A^2 - A_m^2)/\sigma_f^2$, where r, r_m, A, and A_m are the mist-hackle and mirror-mist boundaries and mist-hackle and mirror-mist constants, respectively.

Ravi-Chandar and Knauss[12] observed parabolic markings in the mist and hackle zones that resulted from small flaws that were activated by stresses operating ahead of the main propagating crack and which interacted with the crack front as it advanced. In the hackle zone these markings were generally larger and penetrated deeper into the material below the fracture surface than in the mist zone. It was seen that the maximum depth of the surface markings increased monotonically along the crack path.

We would like to relate the fracture zones to the dynamics of crack propagation. When the rate of the elastic energy liberated by the fracture process (which increases with crack length) becomes greater than that needed for the creation of the two new ''mirror'' surfaces, some energy goes to create small secondary cracks[12] in ''parallel'' to the primary crack. These secondary cracks form the ''mist.''[25] A portion of these secondary cracks grows under the influence of the stress field created by the primary crack until they are ''swallowed up'' by it as it passes them by.[7]

It was shown[26] that further up in the mist zone, the growing secondary cracks become longer before the primary crack overtakes them, and therefore the mist area becomes rougher.[27]

Next, there is a transition to the hackle zone. The existence of such a transition has been questioned recently. In Mecholshy's paper,[28] for example, the mist and hackle regions are described as ''identical in appearance but different in scale.'' Most authors, however, agree[27,29] that a sharp change of form appears at the transition and even Mecholsky[28] concedes that there is an unexplained ''abrupt change'' there. We shall use the conventional approach[29] and try to explain the origin of the different shapes appearing in the mist and hackle zones. We would like to relate the onset of the transition to the Hackle zone to the *inability* of the primary crack to catch up with the secondary cracks, which then grow separately (until they coalesce together at a later stage). For such an interpretation we must have a velocity growth pattern for the secondary cracks that reflects such an inability. As we presently show, for the ''existing'' fracture velocity growth rules, the main crack always overtakes the secondary ones and hence these rules cannot be used under our assumptions. Our suggested new velocity rule fulfills the above requirement and therefore ''explains'' the mist-hackle transition. The check of this rule, however (besides being the obvious first approximation; see below), is in the possibility to use it to derive the shapes of the growing secondary cracks. Experimental evidence strongly supports this rule.

A previous attempt at calculating shapes of secondary fractures in a similar way was undertaken by several authors.[30,31] In these papers, however, the erronous assumption that the secondary cracks move, from their very incipience, with the same final velocity V of the primary crack has led to ''parabolic'' or hyperbolic shapes all through. Such shapes actually appear in the hackle zone and not previously (see below).

Note that a sharp rise in the length of ''secondary cracks,'' possibly, from hackles to branches (bifuraction) was identified at a critical crack velocity $V_c = 0.42 V_R$,[32] where V_R is Reyleigh wave velocity. This range, however, is beyond the scope of the present study.

II. MODEL

A. Velocity rule

Let us start [Fig. 2(a)] from a situation in which at time $t=0$ a secondary crack (here assumed circular and of radius c_0) begins to grow under the influence of the primary crack (which is depicted as semicircular and of radius R at $t=0$ and which is already growing with the final velocity V).

Following a brief treatment of the kinematics of a secondary crack initiation[26,33] and the obtainment thereby of its geometry, we discuss the secondary crack velocity rule and, by using a Griffith-like condition for its propagation, arrive at the definition of the mist-hackle transition.

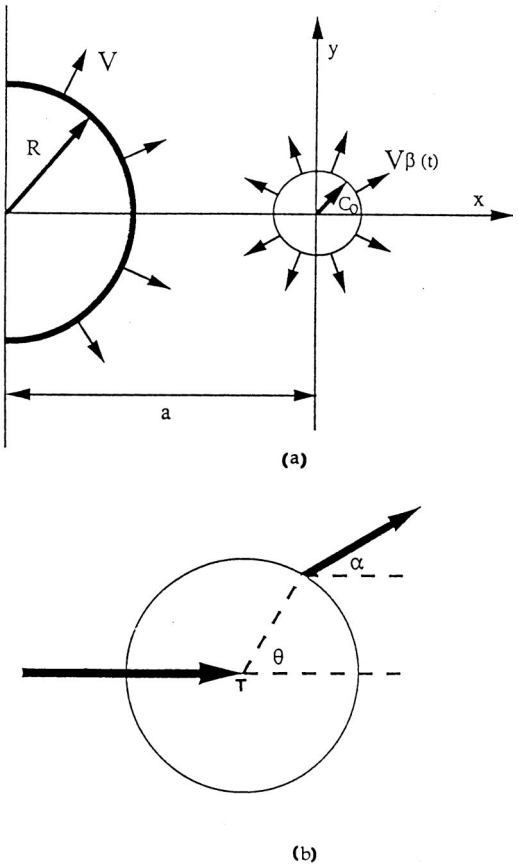

FIG. 2. (a) A schematic picture of the geometrical setup. A secondary crack of length $2c_0$ at a distance a from the origin of the primary crack starts to grow at $t=0$. (b) Side view of the primary crack, T its tip.

Figure 2(b) shows the situation where the primary crack induces a stress field ahead of its tip at the tip of an existing ''flaw'' in the material. The dynamic elastic stress fields σ_{xx}, σ_{yy}, and σ_{xy} in Cartesian coordinates (or the principal stresses σ_1, σ_2) for a mode I crack opening are given by Ref. 33. It is assumed[25] that the flaw would start to grow at an angle θ_1, where the principal maximal stress σ_1 attains its maximum value. Furthermore, the direction of growth of the secondary crack would be at an angle α_1 [Fig. 2(b)] perpendicular to the direction of σ_1 at θ_1.

Neglecting interference from other secondary cracks (shielding) and taking the secondary growth velocity to be given by $V\beta(t)$, the two furthermost points, that of the main crack and that of the secondary one (along the x direction), are, respectively, given by $x_1 = R - a + Vt$ and

$$x_2 = c_0 + V\int_0^t b(t')dt'.$$

A *necessary* condition that there exist a possibility that the primary crack is ''unable to overtake'' the secondary one is that

$$\int_0^\infty [1-\beta(t')]dt' < \infty.$$

In order that the integral does not diverge, the integrand should approach zero[34] faster than t^{-1}. Regular velocity ''rules'' for crack growth are of the form[35–37]

$$\beta(t) = \left(1 - \frac{c_0}{c(t)}\right)^{\nu},$$

where the most used ν's are $\frac{1}{2}$ and 1. Evidently, for large t and for any ν, $c(t) \to Vt$, and therefore $1-\beta(t)$ behaves as t^{-1}. This type of a velocity rule is thus inappropriate for secondary crack growth under our assumptions. Although an exact form for the secondary crack velocity is unknown (the secondary crack moves under a changing stress field caused by the primary crack, whose distance from the secondary one is continuously changing, and by the sample's remote stress) the following constraints have to be fulfilled.

(A) The secondary crack should start from zero, i.e., $\beta(0)=0$.

(B) Asymptotically, this velocity should reach V, the final velocity in this material, i.e., $\beta(t\to\infty)=1$.

(C) Since the secondary crack starts to increase in size only after the stress at its tip is above the critical one, its initial acceleration should be positive, i.e., $\partial\beta/\partial t \ (t=0) > 0$.

(D) The necessary ''no overtake'' condition should be possible.

We therefore assume the following velocity growth rule which is a natural first approximation to the actual rule and meets all these constraints:

$$\beta(t) = 1 - \exp\{-\zeta Vt/c_0\}, \tag{1}$$

where ζ is a dimensionless parameter and, as we presently show, is related to the hackle radius.

Note that, according to Eq. (1), the acceleration of the secondary cracks,

$$\dot{v} = \frac{V}{t_0}\zeta \exp\left\{-\frac{t\zeta}{t_0}\right\},$$

where $t_0 = c_0/V$. Thus, in contrast to the primary crack velocity rule for which the initial acceleration is infinite,[37] Eq. (1) yields a *finite* initial acceleration which diminishes exponentially. Equation (1), again in contrast to the primary crack rule, is readily integrable and gives for the secondary crack radius

$$c = c_0 + Vt + \frac{c_0}{\zeta}\left[\exp\left(-\frac{\zeta Vt}{c_0}\right) - 1\right]. \tag{2}$$

B. Relation between *a* and *R*

In order that always $x_1 \leqslant x_2$, we obtain the condition

$$c_0 \leqslant \zeta(a - R + c_0). \tag{3}$$

However, for the secondary crack to commence growing, it is necessary (see Ref. 26 for a full presentation) that the stress intensity factor (SIF) $\sigma_1(\pi c_0)^{1/2}$ at the tip of the flaw be greater than the critical SIF (K_{I_c}). According to Ref. 26, the criterion for the secondary crack to grow is, therefore,

$$\frac{a - R + c_0}{c_0} = (K_I/K_{I_c})^2 f^2 \frac{\cos\theta}{2}.$$

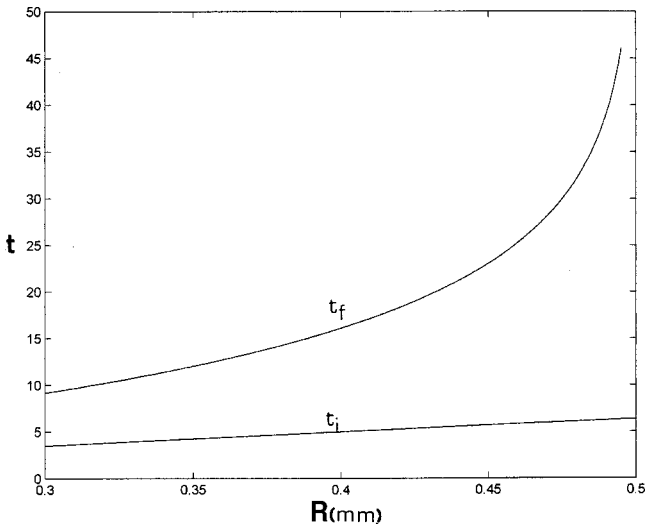

FIG. 3. Initiation t_i and termination t_f times for the SCS in the mist zone, as a function of R (between r_m and r). Numbers relate to the example calculated in Sec. III. Times are measured in units of $t_0 = c_0/V$, and the nondimensional R is measured in units of c_0.

K_I is the SIF of the primary crack, and $f(\theta,v)$ is a geometric factor,[33] of the order of 1. For a constant ζ the combined condition is

$$\zeta \geqslant \frac{2K_{I_c}^2}{K_I^2 f^2 \cos\theta}, \tag{4}$$

with the equality sign occurring for hackle initiation, namely, for $K_I = K_{I_H}$.

Now, K_I is proportional to $\sigma\sqrt{R}$, while K_{I_c} is proportional to $\sigma\sqrt{C_{\rm cr}}$, where $C_{\rm cr}$ is the critical radius of the primary crack and σ is the remote stress causing the primary fracture.

On the other hand, by the discussion following Eq. (4),

$$\zeta = \left(\frac{K_{I_c}}{K_{I_H}}\right)^2 \frac{2}{f^2 \cos\theta}, \tag{5}$$

where K_{I_H} is proportional to $\sigma\sqrt{r}$ where r is the radius of mist to hackle transition (or in short the hackle radius). The criterion (3) thus becomes

$$\frac{a - R + c_0}{c_0} = \frac{R}{\zeta_r}. \tag{6}$$

For $f \approx 1.4$ and for $\theta \approx 0°$,[26] $\zeta r \approx C_{\rm cr}$ [by Eq. (5)].

The relation between a and R is therefore

$$a = R\left[1 + \frac{c_0}{\zeta_r}\right] - c_0 \approx R\left[1 + \frac{c_0}{C_{\rm cr}}\right] - c_0 . \tag{7}$$

The distance L between the leading fronts of the primary and secondary cracks ($L = a - R + c_0$) is a measure of the ''advantage'' the secondary crack has with respect to the primary when it commences to grow. It is given by

$$L \approx R\frac{c_0}{C_{\rm cr}}. \tag{8}$$

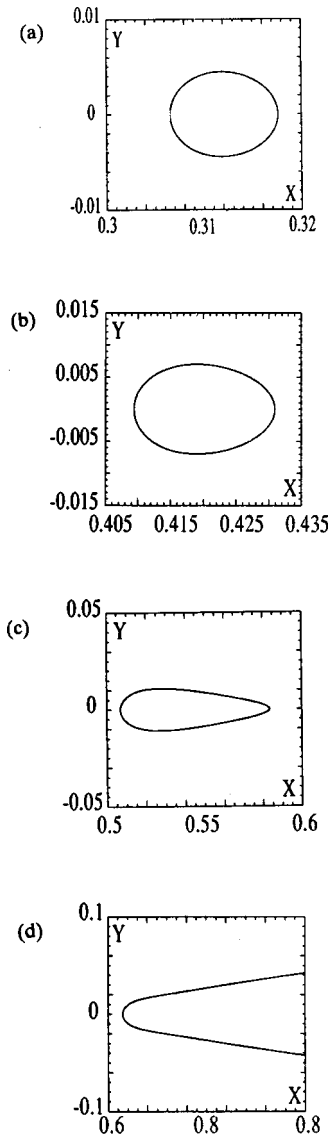

FIG. 4. Calculated shapes of ''final'' secondary cracks in the mist and hackle zones, for different radii of the primary crack (flaw size $c_0 = 0.002$ mm). x and y scales are in mm. (a) $R = 0.3$ mm, the beginning of the mist zone (oval); (b) $R = 0.4$ mm, in the mist zone (elliptic); (c) $R = 0.495$ mm, towards the end of the mist zone (tear drop); (d) $R = 0.6$ mm, in the hackle zone (hyperbolic).

For the range of R values $r_m < R < r$, we get

$$\frac{r_m}{C_{\rm cr}} < \frac{L}{c_0} < \frac{r}{C_{\rm cr}}. \tag{9}$$

Our present interpretation of the hackle initiation process is as follows: all parameters except K_I on the right-hand side of Eq. (4) are constant for a specific material. For a constant stress process, K_I increases in proportion to the square root of the primary crack length. For small primary crack lengths, Eq. (4) is not valid and all secondary cracks are stopped (mist region). Given enough time, K_I keeps increasing until the equality sign of Eq. (4) is reached [Eq. (5)]. At this point, the secondary cracks can no longer be stopped and hackle ensues. Note that for a constant ζ, *all* secondary cracks, irrespective of their initial size, reach the ''hackle condition'' for the same length of the primary

crack.[38] Thus hackle should occur at a well-defined radius r (Fig. 1), a result well supported by experiments.

C. Shapes of secondary cracks

In order to calculate the shapes of the secondary cracks in the mist zone and in the mist-hackle transition region, we use the following well-established model[39] with our velocity rule (see Fig. 2). The secondary crack is initially circular of radius c_0. It grows in a parallel plane[25] to that of the primary one, with the velocity $V\beta(t)$ of Eq. (1). The primary crack, meanwhile, advances with velocity V. A point on the secondary crack, which is ''swept by'' (in parallel to) the primary crack, stops growing since the stress there has relaxed. The ''final shape'' of the secondary crack is therefore given by the intersection of the following two curves:

$$x^2+y^2=(R+Vt)^2,$$

$$(x-a)^2+y^2=\left\{c_0+Vt+\frac{c_0}{\zeta}\left[\exp\left(-\frac{\zeta Vt}{c_0}\right)-1\right]\right\}^2, \tag{10}$$

where a is a linear function of R [Eq. (7)]. This is a parametric formula for the final *shape* of the *secondary crack* (SCS).

A nondimensional form of Eqs. (10) is obtained by measuring lengths (i.e., x,y,R,a) in units of c_0 and the time in units of $t_0=c_0/V$ (a half of the interval it takes the primary crack to cross the length of the secondary flaw). Equations (10) then become

$$x^2+y^2=(R+t)^2,$$

$$(x-a)^2+y^2=\left[1+t+\frac{1}{\xi}(e^{-\zeta t}-1)\right]^2. \tag{11}$$

These equations, with a given by [see Eq. (7) where $a,R,C_{\rm cr}$ are in units of c_0]

$$a=R\left(1+\frac{1}{C_{\rm cr}}\right)-1, \tag{12}$$

constitute a parametric representation of the differenct SCS's. Note that for a specific case ζ is a constant while R changes across the mist zone, from r_m to r, with different ensuing SCS's along the way.

In order to evaluate the times of initiation and termination of the SCS's, intersections of the latter with the x axis are needed. These are given by

$$x=R+t,$$

$$x-a=\pm\left[1+t+\frac{1}{\xi}(e^{-\zeta t}-1)\right]. \tag{13}$$

The minus sign gives the first intersection time, while the plus sign relates to the termination time (when it exists—before hackle sets in). We denote these times as t_i and t_f, respectively.

The termination time t_f is easily calculated from Eqs. (13) to be

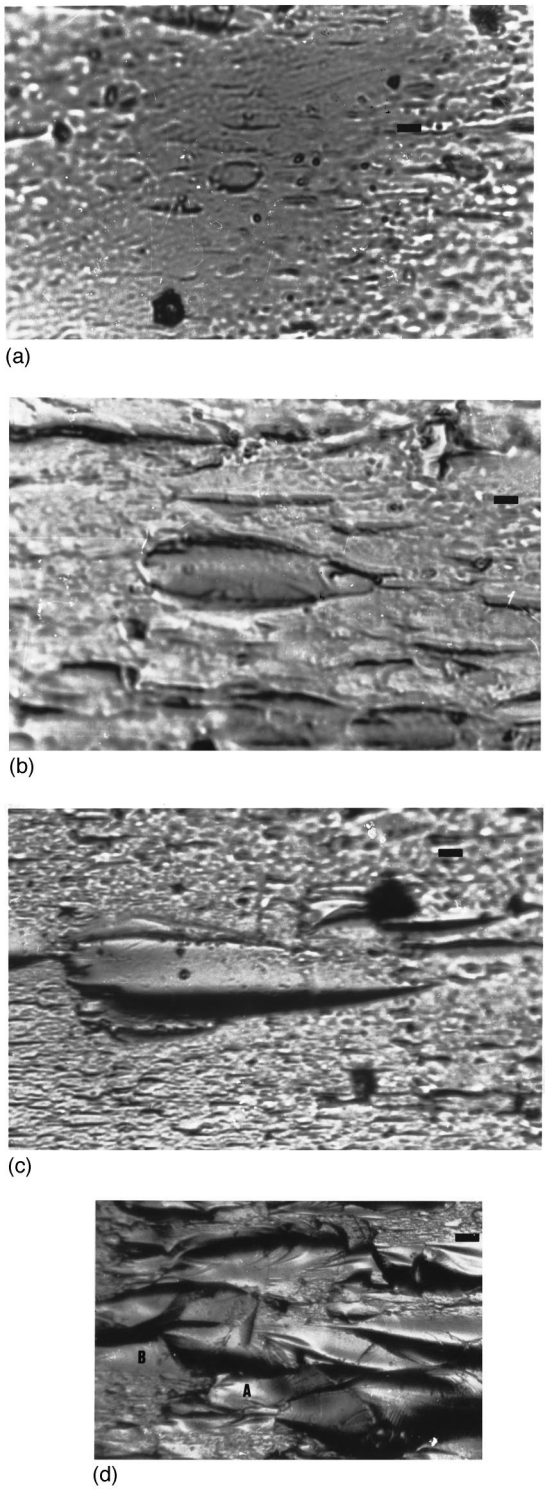

FIG. 5. Experimental results for soda lime glass fracture. (a) The beginning of the mist zone (oval), scale bar 2.5 μm; (b) towards the end of the mist zone (tear drop), scale bar 10.0 μm; (c) at the mist hackle transition (two semiparallel lines), scale bar 10.0 μm; (d) in the hackle zone (neighboring hyperbolic SCS's, e.g., A and B), scale bar 20.0 μm.

$$t_f=-\frac{1}{\xi}\ln\left(1-\frac{R}{r}\right), \tag{14}$$

while t_i can be calculated from

$$2t_i+\frac{1}{\xi}e^{-\zeta t_i}=\frac{R}{R_c}-2+\frac{1}{\zeta}. \tag{15}$$

Results for the case treated below are given in Fig. 3. It seems that while t_i increases slowly with R, mainly due to the increase of the ''advantage'' L,t_f increases very sharply as the hackle is approached and goes to infinity. Since the SCS's are dependent on the t_f-t_i interval and the latter increases monotonously between r_m and r, it is to be expected that, qualitatively, the same SCS's would be obtained for every brittle fracture, albeit at different positions and with different magnitudes.

Denoting $U=R+c_0/\zeta-c_0$, the ''no overtake'' condition (3) is $U\leqslant a$. For the ''exact'' hackle condition $U=a$, Eq. (13) yields the result that the second intersection of the SCS with the x axis occurs at $x\rightarrow\infty$ $(t\rightarrow\infty)$. Physically, it means that at r the SCS develops as two parallel lines.

For $R>r$ the SCS reaches asymptotically a hyperbola. To see this assume that the time is large enough so that the exponent in Eq. (10) or (13) can be neglected. In polar coordinates Eq. (10) is then given by

$$\frac{1}{2}=\frac{2U}{U^2-a^2}(1-\epsilon\cos\theta), \tag{16}$$

where $\epsilon=a/U$ and is >1. This is the equation of a hyperbola with asymptotes $\cos\theta=U/a$. The prefactor is negative, as in the case of scattering from a central repelling force.

Since at this stage the secondary cracks move with a velocity mearly equal to the final one, the treatment of Refs. 30 and 31 becomes asymstotically applicable, and hence the agreement with the hyperbolic shapes here.

III. COMPARISON WITH EXPERIMENTAL RESULTS

To demonstrate the shapes of the SCS, we use the following ''realistic parameters'' for soda-lime glass:[40] $V=1500$ m/sec, $K_H/K_{I_c}\sim 3.1$, and $f\sim 1.4$. The range of the mist zone in this case[40] is $0.3\,\text{mm}\leqslant R\leqslant 0.5\,\text{mm}$. In Figs. 4 and 5 calculated SCS's are compared with experimental results. The calculated SCS's are for the above-mentioned range and for an initial c_0 of 2 μm.[41] Hence $t_0\sim 1.3\times 10^{-9}$ sec, $a\sim 1.04R-2\times 10^{-3}$ (mm), and $L\sim 0.04R$. For the mist zone $r_m<R<r$, we have $12\,\mu\text{m}<L<20\,\mu\text{m}$, $\theta\sim 0°$, $r=0.5$, and therefore, $\zeta=3.1^{-2}\sim 0.1$ and $C_{\text{cr}}\sim\zeta r\sim 50\,\mu$m.

The patterns show the following features. At the beginning of the mist zone ($R\sim 0.3$ mm), the SCS's look like elongated ellipses where the elongation increases with c_0 (thus, for small c_0's, the SCS would resemble circles). Further on in the mist zone, the SCS's start to develop a ''narrowing''[42] pointing towards the hackle zone which turns into a ''tear-drop''-like form later on. At the mist-hackle transition $R\sim 0.5$ mm, the SCS's assume the ''two-parallel-line'' shape.

For $R\sim 0.6$, in the hackle zone, the hyperbolic forms appear, increasing in aperture with c_0.

The calculated SCS's of Fig. 4 are in good agreement with existing experimental results (see, e.g., Ref. 23 for the mist zone) and with our experimental results of the mist and hackle regions shown in Fig. 5 measured for a broader mist zone. Note that observations of ''penny-shaped'' (or circular) secondary cracks are very rare. This is of course due to the fact that flaws are seldom of this shape and their initial orientation is seldom in parallel to the main crack. Since what is measured are the ''projections'' of the SCS's onto the primary fracture plane and since the SCS's change their orientation (in the third dimension) during their growth, a quantitative comparison is very difficult. Qualitatively, however, these results show trends similar to those of Fig. 4: (a) The lengths of the experimental SCS's (see scales in Fig. 5) monotonically increase by similar magnifications as in Fig. 4 across the mist zone. (b) Elongated ellipses appear, developing a ''narrowing'' and eventually assuming hyperbolic features (even though not in the same plane) at the hackle zone.

Note that ''two-parallel-line'' shapes do appear, but (as also happens for the hyperbolic shapes) do not continue for large distances due to various interactions.

This agreement gives support to our model.

For fracture in polymers of relatively high molecular weights, interesting features which look like ''parabolas'' or ''hyperbolas'' appear within the mirror zone.[43] Since these materials exhibit some unique properties, such as strain rate sensitivity, crazes, etc., we expect that this ''untimely'' appearance of the hyperbolic shapes is due to some specific mechanism. One possibility is that, for some flaws in these materials, ζ is not a constant, but achieves high values even in the mirror plane. For these flaws, therefore, K_{I_H} can appear earlier than usual, even in the mirror zone. By far, however, ''the most important and widely observed features of ceramic fracture are the normally sequentially formed mirror, mist, hackle and crack branching patterns.''[28] For these brittle materials, our model should describe the natural sequence of events indicating a constant ζ behavior.

Thus, assuming a simple exponential growth law for the secondary crack velocity, we have obtained both a possible understanding of the SCS's in the mist and hackle zones and a simple explanation of the mist-hackle transition itself. Knowledge of the exact velocity growth rule would provide a better quantitative comparison of shapes and transition points, but the overall qualitative picture should, in our opinion, remain intact.

[1] D. Bahat, *Tectonofractography* (Springer-Verlag, Berlin, 1991), p. 87ff.

[2] F. W. Preston, J. Soc. Glass Technol. **10**, 234 (1926).

[3] L. K. Baker and G. S. Glaesemann, Corning Res. (Corning Inc., Corning, NY, 1998), pp. 93 ff.

[4] J. J. Mecholsky, S. W. Freiman, and R. W. Rice, J. Mater. Sci. **11**, 1310 (1976).

[5] R. W. Rice, in *Fractography of Glasses and Ceramics III*, edited by J. R. Varner, V. D. Fréchette, and G. D. Quinn, [Ceram. Trans. **64,** 1 (1996)].

[6] B. W. Payne and A. Ball, Philos. Mag. **34**, 917 (1976).
[7] J. Congleton and N. J. Petch, Philos. Mag. **16**, 749 (1967).
[8] D. Haneman and E. N. Pugh, J. Appl. Phys. **34**, 2269 (1963).
[9] H. A. Hoff, K. A. Snail, A. A. Morrish, and J. E. Butler, in *Fractography of Glasses and Ceramics II*, edited by V. D. Fréchette and J. R. Varner [Ceram. Trans. **17,** 2117 (1991)].
[10] E. K. Tschegg, J. Mater. Sci. **18**, 1604 (1983).
[11] J. S. Nadeau, J. Am. Ceram. Soc. **57**, 303 (1974).
[12] K. Ravi-Chandar and W. G. Knauss, Int. J. Fract. **26**, 154 (1984).
[13] E. Sharon, S. P. Gross, and J. Fineberg, Phys. Rev. Lett. **76**, 2117 (1996).
[14] D. Hull, J. Mater. Sci. **31**, 1829 (1996).
[15] F. W. Preston, J. Am. Ceram. Soc. **14**, 419 (1931).
[16] A. K. Bhowmick, J. Mater. Sci. Lett. **5**, 1042 (1986).
[17] F. Kerkhof, Glastech. Ber. **48**, 112 (1975).
[18] See, e.g., H. Schardin, in *Fracture*, edited by B. L. Averbach, D. K. Felbeck, G. T. Hahn, and D. A. Thomas (Wiley, New York, 1959), p. 297ff; J. F. Kalthof, in *Dynamic Crack Propagation*, edited by G. C. Sih (Noordhoff, Leyden, 1973), p. 449ff (especially see Figs. 2.21, 2.22, and 2.23a); A. Kobayashi, N. Ohtani, and T. Sato, J. Appl. Polym. Sci. **18**, 1625 (1974).
[19] Recently, molecular-dynamics-type numerical methods have improved considerably and become sophisticated enough for enabling ''atomistic'' calculations of crack propagation. Although the gross features of fracture are thus obtained, no detailed zone description is yet available; see, e.g., S. J. Zhou, D. M. Beazley, P. S. Lomdahl, and B. I. Holian, Phys. Rev. Lett. **78**, 479 (1997) and references therein; A. Nakano, R. K. Kalia, and P. Vashishta, *ibid.* **75**, 3138 (1995); F. F. Abraham, D. Brodbeck, R. A. Rafey, and W. E. Rudge, *ibid.* **73**, 272 (1994).
[20] J. J. Melcholsky and S. W. Freiman, in *Fracture Mechanics Applied to Brittle Materials*, edited by S. W. Freiman (ASTM, Philadelphia, 1979), p. 220ff.
[21] A. Smekal, Naturwissenschaften **15**, 106 (1936).
[22] N. Terao, J. Phys. Soc. Jpn. **8**, 545 (1953).
[23] See, e.g., J. W. Johnson and D. G. Holloway, Philos. Mag. **17**, 899 (1968).
[24] M. J. Ball, D. J. Landini, and R. C. Bradt, in *Fractography of Ceramic and Metal Failures*, edited by J. J. Mecholsky, Jr. and S. R. Powell, Jr. (American Society for Testing of Materials, Philadelphia, 1984), p. 110.
[25] A. Rabinovitch, G. Belizovsky, and D. Bahat, Int. J. Fract. **63**, R25 (1993).
[26] A. Rabinovitch, G. Belizovsky, and D. Bahat, Philos. Mag. Lett. **70**, 277 (1994).
[27] C. Wünsche, F. Rädlein, and G. H. Frischat, Fresenius J. Anal. Chem. **358**, 349 (1997).
[28] J. J. Mecholsky, Jr., in *Qualitative Fractography: An Assessment in Fractography of Glasses and Ceramics II* (Ref. 9), pp. 413–451.
[29] See, e.g., R. W. Rice, in *Fractography of Ceramic and Metal Failures*, edited by J. J. Mecholsky, Jr. and S. R. Powell, Jr. (American Society for Testing of Materials, Philadelphia, 1984), p. 5, and references therein.
[30] A. Smekal, Österr. Ing. Archiv. **7**, 49 (1953); Ir. J. Leeuwerik, Rheol. Acta **2**, 10 (1962); C. E. Feltner (unpublished).
[31] T. Shioya and R. Ishida, in *Dynamic Failure of Materials*, edited by H. P. Rossmanuth & A. J. Rosakis (Elsevier, New York, 1991), p. 351ff.
[32] E. Sharon and J. Finberg, Nature (London) **397**, 333 (1999).
[33] L. B. Freund and R. J. Clifton, J. Elast. **4**, 293 (1974).
[34] See, e.g., R. Courant, *Differential and Integral Calculus* (Blackie, London, 1942), Vol. 1, p. 250ff.
[35] For a discussion, see M. Marder, Physica D **66**, 125 (1993) and references therein.
[36] See, e.g., F. Kanninen and C. H. Popelar, *Advanced Fracture Mechanics* (Clarendon, Oxford, 1985).
[37] A. Rabinovitch, Philos. Mag. Lett. **70**, 231 (1994).
[38] Since the details of the secondary crack's trajectory at $K_I \geqslant K_{I_H}$ do depend on c_0 (see below), a ''scatter'' of r should and does exist experimentally.
[39] This model (see also Refs. 1 and 7) is very good for short times. As seen in Ref. 25, secondary cracks start to grow parallel to the primary one. As the primary crack approaches, the stress field at the secondary crack changes and its trajectory curves.
[40] S. F. Freiman, D. R. Mulville, and P. W. Mast, J. Mater. Sci. **8**, 1527 (1973).
[41] B. R. Lawn, *Fracture of Brittle Solids*, 2nd. ed. (Cambridge University Press, Cambridge, England, 1993).
[42] Other shapes of this form are seen, e.g., in Döll's paper [W. Döll, J. Mater. Sci. **10**, 935 (1975)] for fracture in PMMA of a relatively low molecular weight (Fig. 6 there).
[43] See e.g., K. Matsushige, Y. Sakurada, and K. Takahashi, J. Mater. Sci. **19**, 1548 (1984).